THE JOURNAL OF PHYSICAL CHEMISTRY B

Article

pubs.acs.org/JPCB

Ion Pairing and Dynamics of the Ionic Liquid 1-Hexyl-3-methylimidazolium Bis(irifluoromethylsulfonyl)amide ([C_6mim][NTf_2]) in the Low Dielectric Solvent Chloroform

Nathan T. Scharf,[†] Annegret Stark,[‡] and Markus M. Hoffmann*,[†]

[†]Department of Chemistry, The College at Brockport, State University of New York, Brockport, New York 14420, United States

[‡]Institute for Industrial Chemistry, University of Leipzig, Linnéstrasse 3-4, 04107 Leipzig, Germany

Supporting Information

ABSTRACT: The structural and dynamic behavior of the ionic liquid 1-hexyl-3-methylimidazolium bis(trifluoromethylsulfonyl)amide ([C_6mim][NTf_2]) in chloroform has been studied by experimental measurements of ^{1}H and ^{19}F self-diffusion coefficients, viscosity, and excess molar volume in the concentration range of 0.001−1.0 mol·kg^{-1} and temperatures ranging from 15 to 45 °C. Within measurement uncertainty, the ^{1}H and ^{19}F self-diffusion coefficients are identical at the same experimental conditions of concentration and temperature, indicating that even to the lowest measured concentrations the cation and anion are not completely dissociated. The combined experimental data indicates a progression from ion pairing to aggregate formation as concentration increases where at concentrations near 0.1 mol·kg^{-1} aggregate formation becomes dominant. Concurrently with the formation of the IL aggregates at higher concentrations, we also observe an apparent breakdown of the validity of the Stokes−Einstein equation, which we explain by translational motion to become dominated by individual ion pairs moving rapidly between IL aggregates.

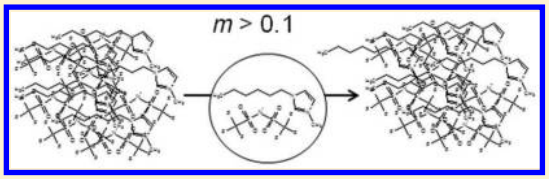

INTRODUCTION

Ionic liquids (ILs) are increasingly explored for a wide variety of applications including, for example, electrochemistry and batteries,[1−5] and as designer solvent media for chemical synthesis.[6−8] ILs are completely composed of ions, usually consisting of an organic cation and some inorganic anion. As a result, not only can the solubility of a wide variety of substances be fashioned into the ionic liquid structure, but unlike regular inorganic salts, ionic liquids can also dissolve appreciably well in a wide variety of conventional organic solvents. This aspect is of importance each time ILs are brought in contact with conventional organic solvents such as for example during the synthesis and purification of ionic liquids. It has been shown that the nature of the anion impacts significantly on the solubility of ionic liquids in other traditional organic solvents. ILs with hard, small anions such as chloride tend to be hydrophilic while ILs with soft, large anions tend to be hydrophobic. As a result, [NTf_2]-type ionic liquids are quite hydrophobic and dissolve substantially in low-dielectric organic solvents. For example, for ionic liquids based on the same cation, the solubility of alkenes such as 1-octene increases in the order of $[BF_4]^-$ < $[PF_6]^-$ < $[CF_3SO_3]^-$ < $[NTf_2]^-$. Similarly, increasing the alkyl chain of the cation substituent has this effect.[9] Once the IL is dissolved in an organic solvent, the presence of ion pairing becomes increasingly more likely at decreasing dielectric constant of the solvent medium as well as other experimental parameters such as decreasing temperature and increasing concentration.[10,11] In fact, in a previous report we noted evidence of very strong ion pairing for the related IL 1-ethyl-3-methylimidazolium bis(trifluoromethylsulfonyl)amide [C_2mim][NTf_2] in chloroform, giving rise to the presence of two separate resonance signals in the proton spectrum.[12] Such two-resonance sets are not observed in [C_6mim][NTf_2] and our initial motivation of this study was to discern if ion pairing is still present. The absence of the two resonance sets could then be due to exchange of cations and anions between freely dissolved and ion paired ions, or to the presence of only either one of these species. To discern this question, we studied the concentration and temperature dependence of the self-diffusion coefficients of both the cation and anion. We expected the diffusion coefficients to plateau at a low enough concentration below which the IL would be completely dissociated. The self-diffusion coefficient, D, of the cation and anion should also differ if the IL is completely dissociated. However, as we will show, even at the lowest concentrations of about 0.001 mol·kg^{-1}, a complete dissociation of the ionic liquid is not indicated. Moreover, from additional independent measurements of viscosity, η, we inspected the concentration dependence of the average hydrodynamic radius, r, of the IL species present in solution that were obtained through use of the Stokes−Einstein equation shown in eq 1

$$D = \frac{k_B T}{c\pi\eta r} \tag{1}$$

Received: May 16, 2012
Revised: August 17, 2012
Published: August 27, 2012

   dx.doi.org/10.1021/jp3047592 | J. Phys. Chem. B 2012, 116, 11488−11497

where k_B is the Boltzmann constant and T is the temperature. The constant c may generally range between 4 and 6 for the so-called slip and stick boundary conditions where there are no interactions between the self-diffusing particle and the surrounding particles for the slip boundary and strong interactions for the stick boundary.[13] The ratio of radii between solute and solvent is also of relevance where for a large solute in a continuum of small solvent c tends to approach the value of 6.[14,15] As we will show, the apparent average hydrodynamic radius for $[C_6mim][NTf_2]$ in chloroform is going through a maximum near 0.1 mol·kg^{-1} concentration and is then decreasing at higher concentration. This finding is of broader importance as there is a renewed interest in studying liquid media that deviate from Stokes−Einstein behavior.[16−20] Additional experimental findings have increased the number of systems where a breakdown of the Stokes−Einstein equation is observed including water and aqueous solutions in the supercooled regime,[21−24] in squalane[25] and cycloalkanes,[26] and nanoparticles in polymer melts[18] as well as ILs and IL-rich systems.[27−31] In these systems there are dynamic heterogeneities present with structural relaxation times differing largely from one spatial domain to the next.[18,32] Recently, the Ludwig group studied carefully the system $[C_2mim][NTf_2]$ in chloroform with molecular dynamics simulation to test the validity of the Stokes−Einstein equation.[29] $[C_2mim][NTf_2]$ has a large solubility gap in chloroform and only very low concentration or very high concentrations of the IL in chloroform could be studied. At low concentrations the IL was found to diffuse according to the Stokes−Einstein equation, but in the IL-rich phase deviations were clearly discerned. In the case of $[C_6mim][NTf_2]$ solubility in chloroform is much higher, and as we will show it appears that an apparent breakdown of the Stokes−Einstein behavior is prevalent at concentrations much lower than what one might have expected.

EXPERIMENTAL SECTION

The $[C_6mim][NTf_2]$ was obtained from Iolitec (CAS no. 382150-50-7, batch no.: G00103.1.1.Inc.) as a clear, colorless substance, with 99% specified purity and was used as received. Its water content was measured by Karl Fischer titration (Denver Instrument) to have a mass fraction of 1.23×10^{-4}. The deuterated chloroform-d (CAS no. 865-49-6) and deuterated dimethylsulfoxide (DMSO-d_6, CAS no. 2206-27-1) were obtained from Acros as 99.98 atom % pure and from Cambridge Isotope as 99.9 atom % pure, respectively. Nondeuterated chloroform (CAS no. 67-66-3) was also used for calibrating the viscometer and for some surface tension measurements, and was obtained from Acros as 99.8% pure. The pure water used for checking calibration of the NMR probe gradient and the density meter was distilled water further purified by a Barnstead UV purification system. The IL solutions were prepared in an inert atmosphere glovebox, then transferred either into a standard 5 mm NMR tube or into a glass syringe (that was then capped) for filling a rolling ball capillary for viscosity measurements as well as a density meter. The NMR sample was freeze−pump−thawed for seven cycles prior to flame sealing the frozen sample under reduced pressure over dry nitrogen.

The NMR diffusion data were acquired on a Bruker Avance 300 instrument using a broadband probe with variable-temperature capability. The maximum gradient strength of 55.6 ± 0.1 G/cm was determined by independent self-diffusion calibration measurements with pure water.[33] The temperature of the broadband probe was calibrated against the known temperature dependence of the chemical shift of neat ethylene glycol[34] and was precise and stable to 0.1 K. Samples were allowed to thermally equilibrate for at least 20 min prior to data acquisition during which the NMR sample tubes were not spun. It is well documented that even slight thermal gradients can lead to thermal convection and thus systematic error in NMR self-diffusion measurements.[35] Specially designed pulse sequences are generally available that minimize error from thermal convection, and we used the double stimulated echo pulse sequence with three spoil gradients originally published by Jerschow and Mueller[36,37] that also minimizes systematic errors from eddy currents. Self-diffusion coefficients, D, were obtained by fitting the stimulated echo intensity I as a function of gradient strength, g, according to eq 2

$$I(g) = I_0 e^{-D\gamma^2 g^2 \delta^2 ((4\Delta - \delta)/\pi^2)} \quad (2)$$

where I_0 is the stimulated echo intensity in the absence of a gradient, γ the gyromagnetic ratio of either fluorine or proton, δ the length of the gradient pulse, and Δ the diffusion time.[38] The gradient pulses were of sine shape and the gradient strength was varied linearly 16 times. Sixteen scans were generally acquired for each gradient strength. At the lowest concentration studied the number of scans was increased up to 32 to increase the signal-to-noise ratio. While the diffusion time was kept fixed at 0.1 ms throughout all diffusion measurements, the length of the gradient pulse was optimized for each sample and ranged between 0.85 ms for the lowest concentration to 2.6 ms for the highest concentration. Delays for gradient recovery and eddy diffusion were set to 0.1 and 5 ms, respectively. ^{1}H and ^{19}F T_1 relaxation times were crudely checked at the highest temperature of 45 °C, where relaxation times are the longest, to ensure that relaxation delays were set to at least three times T_1 for the self-diffusion measurements. The T_1 relaxation times increased with decreasing IL concentration with the highest values at about 6 s for the 0.001 mol·kg^{-1} sample. To illustrate the data quality of the diffusion measurements, a typical plot of $\ln(I)$ against g^2 is shown in Figure S1 of the Supporting Information for the case of the cation H(2) signal from the 0.029 mol·kg^{-1} solution sample at 45 °C. No systematic deviations from linearity at lower gradient strengths are observed, indicating the absence of systematic errors due to thermal convection currents. Since the IL cation shows seven distinct, nonoverlapping lines in the proton spectrum, the standard deviation from the average of the self-diffusion coefficients obtained from each cation proton resonance can be used as a measure of reproducibility, which was within 3.2% of the average value (typically 1%).

Viscosities were measured with a rolling ball viscometer. Since the viscosity measurements require knowledge of densities, these were measured in parallel with a vibrating tube density meter with internal sample viscosity compensation. The AMVn Automated Microviscometer and the DMA 4100 vibrating tube density meter were both manufactured by Anton Paar. Both instruments are temperature controlled to within 0.02 °C by a Peltier system. Since the viscosities of the IL−chloroform solutions were generally lower than that of pure water, the viscometer was calibrated against neat chloroform.[39] Viscosities were measured with a 1.6 mm capillary at an angle of 20° in six repetitions. The reported viscosities are the average values of these repetitions and the standard deviation was

typically less than 1% of the average value. For assessing the accuracy of the measured densities, temperature-dependent density measurements were conducted for pure water in the range of 20−85 °C. The results deviated less than 0.001 g·cm^{-3} from the literature values.[40]

Surface tension measurements were obtained with a Krüss pocket dyne tensiometer that measures the force required to push an air bubble out of a Teflon capillary. The reported surface tension and temperature values are averages and standard deviations of 30−50 measurements repeated about every 1−2 s for several minutes. Measurements were conducted swiftly for each sample to minimize loss of chloroform during measurement due to evaporation.

RESULTS AND DISCUSSION

Self-diffusion. Scheme 1 shows the chemical structure of [C_6mim][NTf_2] and number labels for all chemically distinct

Scheme 1. [C_6mim][NTf_2] with Number Labeling for C/H Sites in Cation

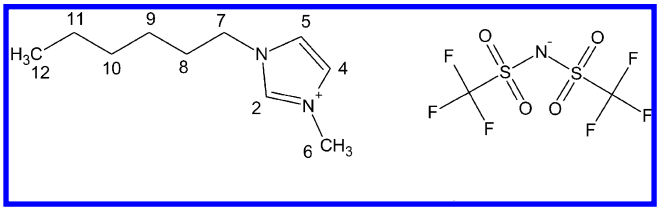

^{1}H/^{13}C sites. In Figure 1 are shown the self-diffusion coefficients of the cation obtained from the ^{1}H-DOSY NMR data and for the anion obtained from the ^{19}F-DOSY data as described in the Experimental Section. The values are also tabulated in Tables S1 and S2 of the Supporting Information. The range of concentrations covered is 0.001 to about 1 mol·kg^{-1}, which expressed in mole fractions of IL corresponds to 1.12 × 10^{-4} to 0.108. Two important observations are immediately evident from Figure 1. First, even to the lowest concentrations at the highest temperature of 45 °C the self-diffusion coefficients do not plateau but keep increasing upon further dilution. Second, the self-diffusion coefficients of the cation and the anion are essentially indistinguishable for the entire investigated concentration and temperature ranges. Both of these observations are indicative that upon dilution of the IL in chloroform the cation and anion do not become completely dissociated but remain significantly ion paired or even aggregated. If they were completely dissociated the cation should self-diffuse measurably slower than the anion due to the larger size of the cation. One would also expect a near concentration independence of the diffusion coefficients if the IL were completely dissociated because the diffusion coefficient would only depend on the increase of fluidity (i.e., the inverse of the solution viscosity) which at low concentrations is only minimally changing. In fact, such behavior has been clearly observed for other IL systems such as, for example, 1-dodecyl-3-methylimidazolium and 1-dodecylpyridinium bromides in water where at a concentration of 0.01 mol·kg^{-1} a relatively sharp transition from gradually increasing self-diffusion-coefficients to concentration-independent self-diffusion coefficients was observed upon dilution.[41]

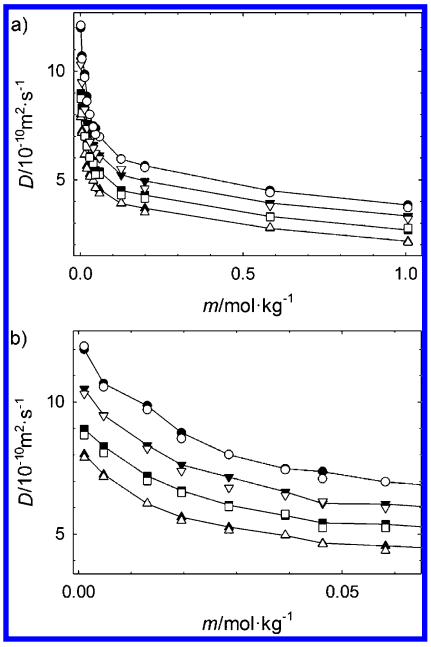

Figure 1. Self-diffusion coefficient for the cation (solid symbols) and anion (open symbols) of [C_6mim][NTf_2] in deuterated chloroform at (△) 15 °C, (□) 25 °C, (▽) 35 °C, and (○) 45 °C; (a) molality range from 0 to 1 mol·kg^{-1}, (b) enlarged molality scale from 0 to 0.065 mol·kg^{-1}.

Viscosity. To actually obtain hydrodynamic radii for the IL cation, r_+, and anion, r_-, by employing the Stokes−Einstein equation, eq 1, independent solution viscosity measurements are needed in addition to the self-diffusion data. These are furnished in Table S3 of the Supporting Information and are shown in Figure 2 covering the same concentration and temperature ranges as for the self-diffusion data. The viscosity data in Figure 2 show near-linear relations in particular at the lowest concentrations and could be fitted with a second-order polynomial $y = a_2x^2 + a_1x + a_0$ to an R^2 value of 0.999. Table 1 summarizes the fitting coefficients and the statistics. Overall,

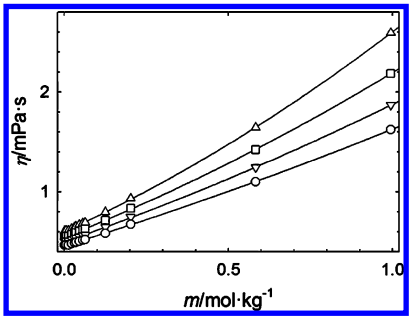

Figure 2. Viscosities, η, for solutions of [C_6mim][NTf_2] in deuterated chloroform at (△) 15 °C, (□) 25 °C, (▽) 35 °C, and (○) 45 °C.

Table 1. Second-Order Polynomial Fitting Coefficients for the Viscosity (in mPa·s) as a Function of Solution Molality of [C_6mim][NTf_2] in $CDCl_3$

coeff	15 °C	25 °C	35 °C	45 °C
a_2	0.1595	0.3388	0.231	0.1595
a_1	1.0117	1.3131	1.1496	1.0117
a_0	0.4578	0.5445	0.4978	0.4578
R^2	0.999	0.999	0.999	0.999
σ/mPa·s	0.0047	0.0042	0.0037	0.0032

dx.doi.org/10.1021/jp3047592 | J. Phys. Chem. B 2012, 116, 11488−11497

the expected trends are observed in Figure 2 insofar that viscosity increases with increasing solution concentration and decreasing temperature.

Hydrodynamic Radii. The fit equations from Table 1 were used to evaluate the solution viscosity at the exact same concentrations for which we have obtained self-diffusion data and were then used to evaluate the hydrodynamic radii r_+ and r_-. As we will compare the calculated radii in several different ways, the radii summarized in Tables S4−S7 in the Supporting Information and in part shown in Figure 3 were calculated

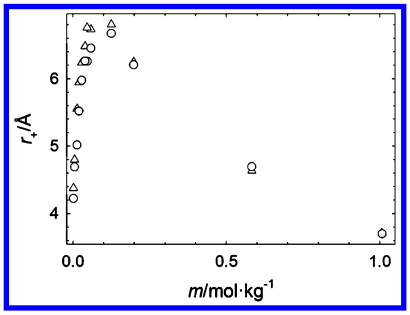

Figure 3. Hydrodynamic radii, r_+, for $[C_6mim][NTf_2]$ in deuterated chloroform at (△) 15 °C and (○) 45 °C obtained from the Stokes−Einstein equation (eq 1) using c = 6 and the experimental data in Figures 1 and 2.

using eq 1 with a value of 6 for c, i.e., using the stick boundary condition. Since the diffusion coefficients of the cation and anion were essentially indistinguishable, as a result so are their radii. In fact, we more carefully checked on this point and refer the reader to the Supporting Information for this discussion.

It is also apparent from Tables S4−S7 of the Supporting Information that the radii are nearly temperature independent. Therefore, we illustrate the concentration dependence of the radii in Figure 3 only for the lowest and highest measured temperature and also only for the cation. Indeed, radii of the cation are only noticeably larger at 15 °C than at 45 °C at concentrations below 0.1 mol·kg^{-1} but essentially indistinguishable for the three higher concentrations near 0.2, 0.6, and 1.0 mol·kg^{-1}.

It is evident in Figure 3 that the radii go through a maximum near 0.1 mol·kg^{-1} and then decrease at higher concentrations. This observation is surprising as we expected the Stokes−Einstein equation to be valid at such concentrations. An increase in concentration should favor the formation of ion pairs and at sufficiently high concentrations possible formation of aggregates, which would possess larger and not smaller hydrodynamic radii. As further detailed in the Experimental Section, we were careful in avoiding systematic errors in the diffusion measurements from thermal convection currents in the sample. Nevertheless, in order to further exclude the presence of systematic experimental error, additional data was acquired for solutions of $[C_6mim][NTf_2]$ but this time in deuterated dimethyl sulfoxide (DMSO-d_6). DMSO is a rather polar solvent and at low concentrations we can assume the IL to be completely dissociated. We also prepared NMR samples using two different containers, a regular 5 mm NMR tube and a sealed melting tube capillary that was placed in a regular 5 mm NMR tube with DMSO to obtain a strong enough lock signal. The inner diameter of the melting tube capillary was 0.8 mm, and convection currents, if present, can be expected to be greatly diminished compared to a standard 5 mm NMR tube. The independent viscosity measurements were obtained using the same sample solutions prepared for the NMR samples. The results and the radii evaluations are shown in Table 2. For the diffusion coefficients of the cation the standard deviation of the average value is included in Table 2 and may be taken as the estimated uncertainty of the self-diffusion coefficient of the anion. The NMR signal obtained from the sample in the melting tube capillary required an increased number of scans in order to obtain reasonable signal-to-noise, 512 as compared to 32 scans for the sample in the regular NMR sample.

Several observations can be made from the results shown in Table 2. The self-diffusion coefficients and thus the radii r_+ and r_- are distinctively different in all DMSO samples, indicating that cation and anion are indeed completely dissociated. Indeed, the obtained hydrodynamic radii r_+ and r_- are each reproducibly of the same value regardless of the two different sample concentrations, NMR sample container, and temperature. They average to 2.97 ± 0.04 Å for r_+ and 2.15 ± 0.08 Å for r_-. Since we obtained the same self-diffusion coefficients for the 0.0089 mol·kg^{-1} solution using the standard 5 mm NMR sample tube and the melting tube capillary, we can exclude systematic experimental error in the obtained self-diffusion coefficients as the source for the apparent reduction in hydrodynamic radii observed in Figure 3 at concentrations larger than about 0.1 mol·kg^{-1}.

So far we have evaluated all radii using the value c = 6 for the stick boundary condition. The cation and anion radii of 2.97 and 2.15 Å in Table 2 would add up to 5.12 Å for the contact ion pair. The value of 5.12 Å matches up surprisingly well with the reported distances of 5.1 Å for the first maximum in the cation−anion center-of-mass radial distribution function

Table 2. Measurements and Evaluations for $[C_6mim][NTf_2]$ in DMSO-d_6

m/mol·kg^{-1}	0.0368	0.0368	0.0368	0.0089	0.0089
NMR sample container	5 mm tube	5 mm tube	5 mm tube	5 mm tube	capillary
T/°C	25	35	45	35	35
$D_+/10^{-10}$ m^2·s^{-1}	3.33 + 0.02	4.14 + 0.05	4.95 + 0.06	4.14 + 0.05	4.19 + 0.08
$D_-/10^{-10}$ m^2·s^{-1}	4.62	5.39	6.77	5.71	6.04
η/mPa·s	2.241 ± 0.004	1.852 ± 0.002	1.563 ± 0.002	1.817 ± 0.001	1.817 ± 0.001
r_+/Å	2.92	2.95	3.01	3	2.97
r_-/Å	2.11	2.26	2.3	2.18	2.06
r_{DMSO}/Å	1.33	1.41	1.37	1.49	1.56
c_+	4.60	4.61	4.65	4.64	4.63
r_{+GW}/Å	3.81	3.83	3.89	3.88	3.85
c_-	4.06	4.18	4.14	4.12	4.02
r_{-GW}/Å	3.11	3.24	3.19	3.17	3.07

dx.doi.org/10.1021/jp3047592 | J. Phys. Chem. B 2012, 116, 11488−11497

obtained from molecular modeling,[42] and in the X-ray weighted cation−anion radial distribution function[43] both for the neat IL $[C_6mim][NTf_2]$. Interestingly, a distance of 5.2 Å for the first maximum in the cation−anion geometrical center radial distribution function was obtained also for $[C_4mim][PF_6]$ from molecular dynamics simulation.[44] However, the hydrodynamic radii for the cation and anion in Table 2 appear to be smaller than what would seem physically reasonable. The Stokes−Einstein equation with $c = 6$ is based on the model of a sphere moving through a viscous medium. The viscosity of DMSO is comparably low, and deviations from the stick boundary conditions can be expected.[45,46] Additional considerations such as the relative size of solute to solvent and shape of diffusing particle would also need be considered for determining accurate radii as recently thoroughly reviewed by Macchioni et al.[15] In this regard, we like to point out that the $[NTf_2]^-$ anion can undergo conformational changes along the CSNS dihedral angle,[47,48] and Tsuzuki et al. report significant decreases in self-diffusion coefficients if the torsional angles are constrained.[49] To account for the relative size of solute radius r and solvent radius r_{solv}, Chen and Chen[50] used eq 3 to evaluate c, which they derived from the microfriction theory by Gierer and Wirtz.[51]

$$c = \frac{6}{\left[1 + 0.695\left(\frac{r_{solv}}{r}\right)^{2.234}\right]} \tag{3}$$

The values for c and r were obtained iteratively through eqs 1 and 3 until they converge using the DMSO van der Waals radius of 2.63 Å that has been shown to agree well with the hydrodynamic radius of neat DMSO-d_6.[52] The resulting values are listed in Table 2 for the cation (c_+, r_{+GW}) and the anion (c_-, r_{-GW}). The average radii for cation and anion of 3.85 and 3.16 Å, respectively, are comparable to reported values in the literature that range from 3.55 to 3.88 Å for the cation and 3.17 to 3.80 Å for the anion.[53−55] (For provided van der Waals volumes, the radii were evaluated using the volume equation of a sphere. For the data from the group of Conboy,[53] the van der Waals volume of the cation was extrapolated from the provided volumes for the shorter chained homologues that increased incrementally by 24 Å^3 per additional $-CH_2-$ group.)

We also recalculated the hydrodynamic radii r_+ and r_- for the IL−chloroform solutions using eqs 1 and 3 and list them in Table S8 in the Supporting Information. The radii increase between 7% for the largest radii and 22% for the smallest radii but the main observation from Figure 3 that the average hydrodynamic radius goes through a maximum at about a 0.1 mol·kg^{-1} concentration remains. Even if one allows for some additional space between anion and cation, the maximum radius value of about 7 Å (or 7.5 Å when using corrected value) observed in Figure 3 would appear to exceed the contact ion pair radius by at least more than 1 Å. Therefore, it seems reasonable to assume that the equilibrium species present at concentrations from 0 to 0.1 mol·kg^{-1} not only include the freely dissolved ions and the contact ion pair but also aggregate species, and at concentrations larger than about 0.05 mol·kg^{-1} where the radii become larger than the added radii of cation and anion, no freely dissolved species are present. The aggregates may either be larger in aggregate number but fewer in concentration or smaller in aggregate number but more concentrated. No distinction can be made in this respect from the data because the radii shown in Figure 3 represent the time and ensemble average radii of all present species. However, given the observation that cation and anion radii are the same even at the chloroform solution concentration of 0.001 mol·kg^{-1}, we can state that the freely dissolved ions are not the dominant species, but the ion pairs and/or aggregates are the dominant equilibrium species present in solution. On the other hand, some amount of freely dissolved cation and anion must be present at the low concentrations because the obtained radii in Figure 3 at these concentrations are smaller than the added radii of the freely dissolved cation and anion.

Although we cannot discern directly from our data how large the aggregates are and how many cations and anions are on average entailed in the aggregates, we can at least attempt some estimations. Taking 7.0 Å as a lower bound and 7.5 Å as an upper bound value would result in aggregate spherical volumes between 1,437 and 1,767 Å^3, respectively. Assuming the aggregates to be charge neutral we can now calculate the maximum number of (spherical) cation and anions that could fit in these volumes based on the radii of cation (3.85 Å = >239 Å^3) and anion (3.16 Å = >132 Å^3). These result in 3.87 IL units for the lower bound and 4.76 IL units for the upper bound that could be fit into the available spherical aggregate volume. These values would therefore allow for the presence of quadrupolar and possibly some higher aggregates, which would be in line with the results from several other investigations. From a Hyper-Rayleigh scattering investigation in several neat ionic liquids a preference for octapolar clusters has been indicated.[56] Such scattering type experiments would in this regard be very helpful to refine the aggregate speciation present. The Wasserscheid group also obtained aggregation numbers of up to about 8 for a particular chiral ionic liquid in dichloromethane.[45] Evidence for the formation of ion quadrupoles has also been observed for other salts in solvents having a relative permittivity of chloroform or lower.[15]

Activation Energy. Since we have temperature-dependent data, we inspected how the Arrhenius activation energy, E_a, as defined in eq 4, for the self-diffusion of the cation (D_+) and anion (D_-) as well as for the fluidity ($1/\eta$) might change with solution concentration.

$$X(T) = Ae^{-E_a/RT} \tag{4}$$

In eq 4, $X(T)$ is the temperature-dependent property (D_+, D_-, or $1/\eta$), A is the pre-exponential factor, and R is the gas constant. The activation energies were obtained from the slopes of plots of $\ln(X)$ against $1/T$ that were generated for each fixed solution concentration. Although the R^2 values of the linear regressions were generally higher than 0.99, in the case of the self-diffusion data the uncertainty of the slope and thus the uncertainty of the resulting activation energies varied widely between 0.1 and 1.4 kJ mol^{-1}. The activation energies and their uncertainties are summarized in Table S9 in the Supporting Information and are plotted against IL mass fraction, c_{IL}, in Figure 4. Mass fractions were chosen as the concentration unit in Figure 4 because, as can be seen in Figure 4, the activation energy for the fluidity is linearly dependent on mass fraction. The linear fit equation $E_a = 16.405c_{IL} + 6.834$ to the fluidity activation energy data results in an R^2 value of 0.9994. The activation energy data in Figure 4 from the self-diffusion data shows more scatter (exemplary error bars are included for the data points of the three highest concentrations) which prevents any firm conclusions. Nevertheless, it appears that the activation energies for the self-diffusion (a) is similar for the cation and anion, (b) is concentration independent for mass

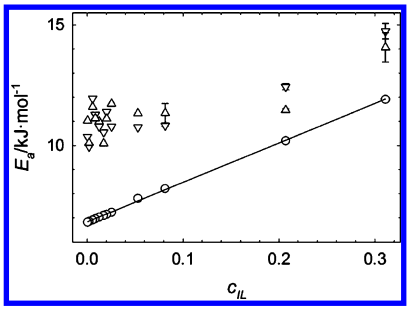

Figure 4. IL mass fraction, c_{IL}, dependent Arrhenius activation energies for (▽) the self-diffusion coefficient of the cation; (△) the self-diffusion coefficient of the anion; and (○) the fluidity ($1/\eta$). The solid line is the linear fit equation $E_a = 16.405c_{IL} + 6.834$ to the fluidity data.

fractions smaller than 0.1, and (c) increases with increasing mass fractions higher than 0.2 possibly with similar slope as for the fluidity activation energy.

It would make sense that activation energy is concentration independent for the self-diffusion at low concentrations if one envisions the translational motion of the freely dissolved and ion paired ions as individual particles floating through a sea of chloroform solvent. At sufficiently high concentration, however, their translational motion will also increasingly be hindered by other ion pairs and/or aggregates. As for the fluidity of the bulk solution, the resistance of shear increases with the increase of the average cohesive forces between particles that can be expected with the addition of the IL to the chloroform solution. It is interesting though that the concentration dependence of activation energy is linear with mass fraction as opposed to other concentration units such as molality or mole fraction. In fact, for the binary system of water in the IL $[C_2mim][MeSO_3]$ we previously observed a linear dependence of the fluidity with water mole fraction, x_w, in the range of $0 < x_w < 0.9$.[30]

Surface Tension. To see if we could obtain evidence for the possible onset of aggregation at molalities higher than about 0.1 mol·kg^{-1}, we made some cursory surface tension measurements of three solutions of $[C_6mim][NTf_2]$ in chloroform, two below and one above 0.1 mol·kg^{-1}. The results are shown in Table 3 and indicate that the surface tension stays unaffected by

Table 3. Surface Tension for Solutions of $[C_6mim][NTf_2]$ in $CHCl_3$

m/mol·kg^{-1}	T/°C	σ/mN·m^{-1}
0.038	25.1 ± 0.2	26.4 ± 0.1
0.071	27.1 ± 0.4	26.1 ± 0.2
0.190	27.1 ± 0.9	26.3 ± 0.2

the increasing IL concentration, at least within our measurement uncertainty, and are essentially the same as the surface tension of 26.67 mN·m^{-1} for neat chloroform at 25 °C.[40] For comparison, the surface tension of neat $[C_6mim][NTf_2]$ at 25 °C has been reported to be near 32 mN·m^{-1}.[57−60] We therefore did not pursue any further surface tension measurements. Apparently, the IL does not populate the surface to any significant extent but prefers to reside in the chloroform bulk. In this regard, it would be of interest to inspect additional data that could be indicative of the interactions present between the IL and chloroform. To this effect, we inspect in the following two subsections additional density data that were obtained as part of the solution viscosity measurements as well as ^{1}H chemical shift data.

Excess Molar Volume. The excess molar volume, V^E, is obtained from density data as shown in eq 5 where the square brackets illustrate that V^E is defined as the difference between the real solution volume and the ideal solution volume, which is the sum of the volumes of the pure components.

$$V^E = \left[\frac{x_{IL}M_{IL} + x_{CDCl_3}M_{CDCl_3}}{\rho}\right] - \left[\frac{x_{IL}M_{IL}}{\rho_{IL}} + \frac{x_{CDCl_3}M_{CDCl_3}}{\rho_{CDCl_3}}\right] \quad (5)$$

In eq 5, x is the mole fraction, M the molar mass, and ρ the density. Table S10 in the Supporting Information contains the directly measured density data including pure $CDCl_3$. To obtain V^E the density of the pure IL is also needed. There are a number of literature values available for the temperature dependence of density of neat $[C_6mim][NTf_2]$.[61−67] We plotted these available data points and obtained a linear fit equation of $\rho_{IL} = 1.6417 - 0.9074 \times 10^{-3}T$, where T is entered in units of Kelvin. The resulting V^E values are summarized in Table S11 in the Supporting Information and are shown in Figure 5. The parameters for the polynomial fit lines shown in

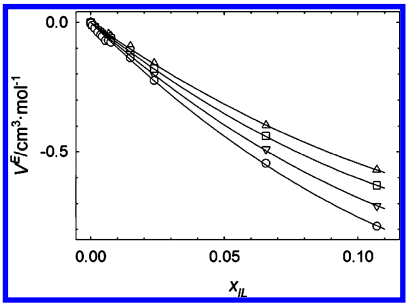

Figure 5. Excess molar volumes as function of mole fraction of the ionic liquid $[C_6mim][NTf_2]$ in $CDCl_3$ at (△) 15 °C, (□) 25 °C, (▽) 35 °C, and (○) 45 °C.

Table 4. Polynomial Fit Parameters to V^E Data in Figure 5

coeff	15 °C	25 °C	35 °C	45 °C
a_2	17.331	20.359	22.893	25.553
a_1	−7.1755	−8.058	−9.0577	−10.071
a_0	0	0	0	0
R^2	0.9982	0.9986	0.9983	0.9988
σ/cm^3·mol^{-1}	0.007	0.007	0.008	0.008

Figure 5 are summarized in Table 4. The excess molar volumes are all negative, which means the volume contracts upon mixing the IL into the neat $CDCl_3$. The solubility of $[C_6mim][NTf_2]$ is much larger compared to $[C_2mim][NTf_2]$ of which less than 0.03 mol·kg^{-1} can dissolve. The interactions between the $[C_6mim][NTf_2]$ and $CDCl_3$ must therefore significantly involve the hydrophobic aliphatic side chain. The interactions between the IL and $CDCl_3$ must be sufficiently strong to penetrate and reorganize the $CDCl_3$ solvent structure. In this regard, it is remarkable that the magnitude of V^E increases with increasing temperature. However, this observation has also been made for the V^E of $[C_6mim][NTf_2]$ in binary systems with a number of

dx.doi.org/10.1021/jp3047592 | J. Phys. Chem. B 2012, 116, 11488−11497

other molecular solvents including dichloromethane, and this observation is apparently not unique to the $[C_6mim][NTf_2]$–$CDCl_3$ binary system.[68] One possible explanation is that with increasing temperature the solvent structure can more easily be broken apart allowing the IL more readily to penetrate and reorganize the solvent structure thus reducing the overall amount of occupied space.

Proton Chemical Shifts. When we began our NMR experiments for this study, our primary focus were the NMR diffusion measurements and less the information on chemical shifts. The $CDCl_3$ used did not include TMS as chemical shift standard nor did we have an external chemical shift standard as part of the NMR sample. The residual proton of $CHCl_3$ from the deuterated chloroform solvent should not be used as chemical shift reference because it can be expected to interact with the ionic liquid. This leaves the chemical shift of the terminal methyl protons of the aliphatic side chain as an alternative, more convenient chemical shift reference option. In an aggregation study of several ILs in water, the chemical shifts of the aliphatic side-chain protons were changing by about 0.1 ppm between the dissociated state and the aggregated state.[69] Since water is much more polar than chloroform, the chemical shift difference between the dissociated and ion paired/aggregated state is likely to be significantly smaller than 0.1 ppm for the aliphatic side-chain protons. Thus, the concentration-dependent ^1H chemical shift data for $[C_6mim][NTf_2]$ in $CDCl_3$ at the four investigated temperatures of 15, 25, 35, and 45 °C that are assembled in Tables S12–S15 in the Supporting Information are all referenced relative to the resonance of the terminal methyl protons. The $CHCl_3$ residual resonance was visible in the proton spectra except for the concentrations of 1.007 and 0.013 mol·kg^{-1} where the chloroform peak overlapped completely with the H4 and H5 resonances. For the spectra of these concentrations we extra- and interpolated the chloroform position in the spectrum from the chemical shift difference relative to the C6 protons. At the lowest concentrations of 0.001 and 0.005 mol·kg^{-1} the $CHCl_3$ residual resonance was actually more intense than the H4 signal with which it overlapped and we could thus not determine the H4 chemical shift value at these concentrations. The concentration dependence of the ^1H chemical shift is qualitatively the same for all four temperatures, and in Figure 6 we show the exemplary data at 25 °C. To better illustrate how the chemical shift changes are observed in the spectra, we included in Figure 6 the proton spectrum for the 1.007 mol·kg^{-1} IL solution and chose the *y*-axis to represent the IL molality. The spectral assignment is provided as part of the figure caption. We note that the signals from H4 and H5 near 7.3 ppm are very close to each other and are overlapping with the chloroform peak, which is thus not included in Figure 6 to avoid clutter. Instead, the chloroform chemical shift will be discussed separately.

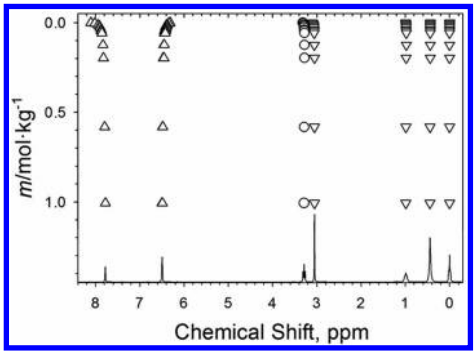

Figure 6. Proton spectrum of 1.007 mol·kg^{-1} solution of $[C_6mim][NTf_2]$ in $CDCl_3$ and chemical shift changes with IL concentration at 25 °C: (△) aromatic protons (from left to right) H2, H4, and H5 (H4 and H5 overlap); (○) H6; (▽) protons of aliphatic side chain (from left to right) H7, H8, H9–H11, H12.

It is immediately evident in Figure 6 and Tables S11–S14 in the Supporting Information that the aromatic ring protons H4 and H5 as well as the $CHCl_3$ proton move to higher chemical shift values (more deshielded) with increasing concentration while all other protons move to lower chemical shift values (more shielded) with increasing IL concentration. We also evaluated the difference in chemical shift between various cation protons and the $CHCl_3$ proton. The results for the H4 and H5 chemical shifts as a function of solution concentration are shown in Figure 7 where it is evident that the chemical shift

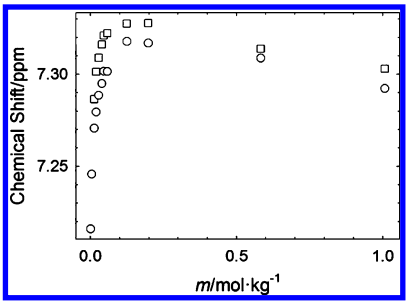

Figure 7. Chemical shift differences between (□) H4 and $CHCl_3$, and (○) H5 and $CHCl_3$ with increasing solution concentration of $[C_6mim][NTf_2]$ in $CDCl_3$.

difference to chloroform for H4 and H5 increases only to about 0.1 mol·kg^{-1} concentration and then slightly decreases again at higher concentration. This trend change is only observable for the H4 and H5 signals but not for the other protons, although the amount of chemical shift difference relative to $CHCl_3$ decreases per concentration unit at concentrations larger than about 0.1 mol·kg^{-1} compared to the concentration range of 0–0.1 mol·kg^{-1}. Although the temperature dependence of the chemical shifts is rather small, as can be seen in Tables S11–S14, the chemical shift difference between H4 and H5 relative to chloroform shows also an opposite trend compared to the other protons with changing temperature.

One possible structural explanation why the chemical shifts of the H4 and H5 relative to chloroform are in opposite trend with increasing IL concentration up to about 0.1 mol·kg^{-1} compared to the chemical shifts of the other protons relative to chloroform could be that the H1 proton interacts with the chloroform through a specific hydrogen-bonding interaction while the interactions between the cation and anion in the ion pair are more purely of Coulomb type involving the cation plus charge distributed over the imidazolium ring and thus affecting all three imidazolium ring protons.

In an earlier study on $[C_2mim][NTf_2]$ in $CDCl_3$, the presence of two resonance sets was observed in the proton spectrum.[12] One of these resonance sets was assigned to the freely dissolved cation, while the other was assigned to the ion-paired species. The chemical shifts for H4 and H5 were observed to be larger by 0.10 and 0.07 ppm for the ion paired species than for the freely dissolved cation, while for all other

dx.doi.org/10.1021/jp3047592 | J. Phys. Chem. B 2012, 116, 11488–11497

resonances the chemical shifts were smaller for the ion paired species, by 0.26 ppm for H1, 0.05 ppm for H7 of the aliphatic side chain, and 0.07 ppm for H6. These chemical shift differences match relatively well the chemical shift differences in Tables S11−S14 in the Supporting Information between the lowest concentration and 0.06 mol·kg^{-1}. Therefore, the chemical shift information corroborates the interpretation of Figure 3 that at concentrations below 0.1 mol·kg^{-1} the chemical equilibrium is dominated by the ion-paired species with increasing amounts of freely dissolved ions present toward the lowest concentrations studied. In this regard, the overall resemblance of Figure 7 to Figure 3 is striking and further suggests that at about 0.1 mol·kg^{-1} concentration higher IL aggregate species are dominant.

Apparent Breakdown of the Stokes−Einstein Equation. Prior experimental and theoretical research has led to the accepted understanding that the breakdown of the Stokes−Einstein equation occurs in systems where structural relaxation times differ widely from spatial region to spatial region.[18,29,32] These systems that are referred to possess spatially heterogeneous dynamics tend to involve solutes that are equal to or smaller than the solvent in size and exhibit local viscosities that differ from the overall bulk viscosity such that the effective hydrodynamic radius lies outside what eq 1 would allow for. The breakdown of the Stokes−Einstein equation has been observed for neat ILs[27,28] as well as for binary systems rich with IL[29,30] displaying a temperature dependence of the self-diffusion coefficients that deviates significantly from eq 1. In the case of $[C_2mim][NTf_2]$ in $CDCl_3$, which is closely related to our studied system, Köddermann et al. find from MD simulations that the time correlation function for the probability of finding the center of mass of cation or anion at some distance from its location at time equals zero is non-Gaussian even when chloroform is added to the IL up to its solubility limit of about 50 wt % indicating the presence of spatially heterogeneous dynamics. Their obtained effective radii for cation and anion were temperature dependent, which they relate to increased heterogeneities at lower temperatures. However, in this study we see an apparent breakdown of the Stokes−Einstein equation at IL concentrations higher than about 0.1 mol·kg^{-1} that corresponds to an IL mole fraction of only 0.01, which is surprisingly low. The obtained radii in Figure 3 are also nearly temperature independent. If we then assume the Stokes−Einstein equation to be principally still valid at these rather low IL concentrations then we must find reasonable explanations for observing a decrease in the average radius of the IL aggregate. Simple redissolution of the ion pairs and aggregates at these low concentrations would seem to be not plausible. The relative permittivity of $[C_6mim][NTf_2]$ should be near 15 according to the data reported by the Weingärtner group of lower homologues of this IL[70] and would anyway contribute insignificantly to the bulk solution dielectric at such low mole fractions. In another study by the same group and co-workers, their conductivity data of related ILs seem to preclude a redissolution of the IL in such a low dielectric solvent as chloroform at such low concentrations.[71] Moreover, even in methanol there appears to be significant ion pair formation of $[NTf_2]^-$-type ionic liquid at IL mole fractions of 0.03 based on small angle scattering data and ^1H and ^{13}C chemical shift data.[72] Likewise, a large degree of ion association has also been observed for chiral ionic liquids in ethanol.[73] The group of Abbott used a model of jumplike motions between vacancies that was originally developed for glass formers.[74] However, this model would also not help in explaining the observed radius maximum in Figure 3 because the radius for the hole r_H according to eq 6

$$r_H = (3.5kT/4\pi\gamma)^{1/2} \quad (6)$$

is dependent on the surface tension, γ, which we have shown to be constant over our studied concentration range. Thus, according to eq 6 r_H is for the studied IL−chloroform system only temperature dependent and amounts to values between 2.05 Å at 15 °C and 2.16 Å at 45 °C.

The fact that we observe deviations from the Stokes−Einstein equation invokes the necessity for a translational mass transport mechanism that differs from the picture of a particle of well-defined radius diffusing through a homogeneous medium. An important consideration here might be the temporal dynamics of the present species. Even entire micelles in aqueous surfactant systems are known to decay and re-form in milliseconds.[75] For the related IL $[C_2mim][NTf_2]$ in chloroform we observed in a prior study two proton NMR resonance sets for the freely dissolved cation and the ion-paired cation, indicating an unusually long lifetime stability of the ion pair of greater than 0.01 s. Although, we do not observe such two-proton NMR resonance sets for $[C_2mim][NTf_2]$ in chloroform, the average lifetimes of the ion pair may still be rather long, meaning that ion exchange between ion pairs is very slow. Ion exchange between quadrupolar and octupolar aggregates may still be relatively slow, but larger aggregates may be less stable and trade ions more easily. In addition, as the aggregate size increases the number of solvent molecules in the surrounding solvation shells increases as well and scales with the aggregate volume, which is $\sim r^3$. If we calculate the available volume for the first solvation shell as the spherical surface layer having a thickness twice the van der Waals radius of chloroform, this would result in a value of 6090 Å^3 for an aggregate of 7 Å radius. From the molar volumes of chloroform each solvent molecule occupies on average about 135 Å^3 resulting in about 45 chloroform molecules in the first solvation shell. For the second solvation shell, the number would increase to about 180. The corresponding mole fraction of IL where we observe the maximum radius size in Figure 3 is about 0.01 which would mean that there are 400 chloroform molecules for each aggregate having an estimated average aggregation number of four. This shows that on average the IL aggregates are actually only separated from each other by about five solvent layers. It is therefore conceivable that translational mass transport of individual ion pairs and lower aggregates moving intact through the chloroform medium changes to a scenario where translational mass transport is dominated by ion pairs jumping fast from aggregate to aggregate. In principle, individual ions instead of or in addition to ion pairs may move as well from aggregate to aggregate. However, the fact that the self-diffusion coefficients of cation and anion remain within measurement uncertainty the same up to the highest investigated solution concentrations seems to support that mainly ion pairs and not individual ions are involved in the mass transport from aggregate to aggregate. Another way to look at this description is that the chloroform solution becomes saturated with lower aggregates when the concentration exceeds 0.1 *m*. Any further addition of ionic liquids does not lead to formation of yet larger aggregates but in effect increases the number of ion pairs such that the average radius of all present IL species decreases.

dx.doi.org/10.1021/jp3047592 | J. Phys. Chem. B 2012, 116, 11488−11497

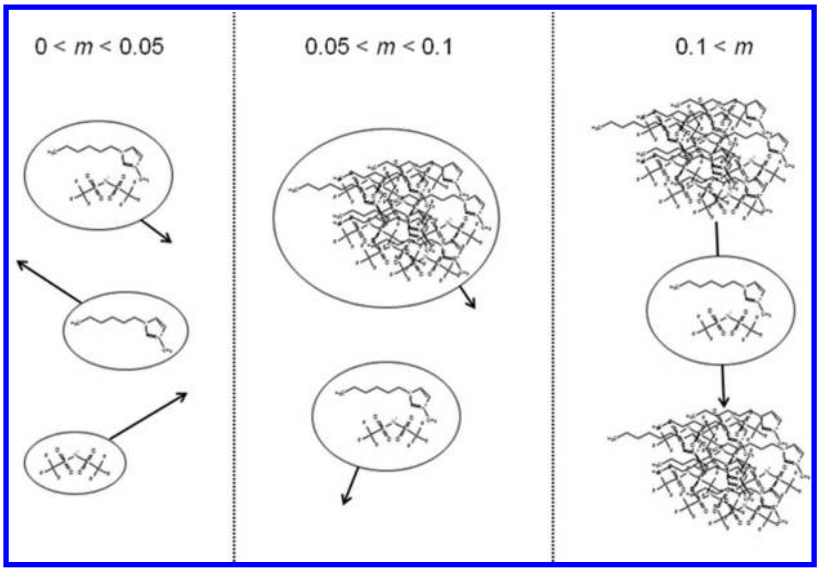

Figure 8. Schematic presentation of the equilibrium speciation and dynamics present for $[C_6mim][NTf_2]$ in $CDCl_3$. At a molality, m, smaller than 0.05, equilibrium mainly concerns ion pairs and some freely dissolved ions, each moving on their own through the chloroform solvent medium. For $0.05 < m < 0.1$ aggregates are formed as well and freely dissociated ions may essentially be absent. For $m > 0.1$ aggregation is dominant but mass transport occurs primarily through ion pairs jumping frequently from aggregate to aggregate.

A pictorial presentation of our main findings and our hypothesis is shown in Figure 8. For molalities smaller than at least 0.05, equilibrium mainly concerns ion pairs as the predominant species and some freely dissolved ions, each moving on their own through the chloroform solvent medium. For $0.05 < m < 0.1$ aggregates are formed as well and freely dissociated ions may essentially be absent. For $m > 0.1$, aggregation is dominant but mass transport occurs primarily through ion pairs jumping frequently from aggregate to aggregate.

CONCLUSION

In summary, we have shown that ion pairing of the IL $[C_6mim][NTf_2]$ is prominent in $CDCl_3$ even to as low concentrations as 0.001 mol·kg^{-1}. At concentrations of about 0.1 mol·kg^{-1}, higher aggregates are formed to significant amounts. Concurrently, we also observe an apparent breakdown of the validity of the Stokes–Einstein equation at these concentrations. To explain the apparent breakdown of the Stokes–Einstein equation, we hypothesize that translational motion at these conditions becomes dominated by individual ion pairs moving relatively rapidly between IL aggregates. Additional studies such as scattering experiments and MD simulations are needed to test and further refine this hypothesis.

ASSOCIATED CONTENT

Supporting Information

The raw experimental data in addition to the data shown in the figure material is available in tabulated form. This material is available free of charge via the Internet at http://pubs.acs.org.

AUTHOR INFORMATION

Corresponding Author

*E-mail: mhoffman@brockport.edu. Phone: 585-395-5598. Fax: 585-395-5805.

Notes

The authors declare no competing financial interest.

ACKNOWLEDGMENTS

This report is based upon work supported by the National Science Foundation under RUI-Grant No. 0842960 (to M.M.H.) and DFG STA1027/2-3 (to A.S.).

REFERENCES

(1) Abbott, A. P.; Ryder, K. S.; Konig, U. *Trans. Inst. Met. Finish.* **2008**, *86*, 196–204.
(2) MacFarlane, D. R.; Pringle, J. M.; Howlett, P. C.; Forsyth, M. *Phys. Chem. Chem. Phys.* **2010**, *12*, 1659–1669.
(3) Armand, M.; Endres, F.; MacFarlane, D. R.; Ohno, H.; Scrosati, B. *Nat. Mater.* **2009**, *8*, 621–629.
(4) Endres, F., Abbott, A. P., MacFarlane, D., Eds. *Electrodeposition Ionic Liquids*; Wiley-VCH: Weinheim, Germany, 2008; pp 369–377.
(5) Liu, H.; Liu, Y.; Li, J. *Phys. Chem. Chem. Phys.* **2010**, *12*, 1685–1697.
(6) Chaturvedi, D. *Curr. Org. Synth.* **2011**, *8*, 438–471.
(7) Koel, M. *Ionic Liq. Chem. Anal.* **2009**, 397–399.
(8) Moniruzzaman, M.; Nakashima, K.; Kamiya, N.; Goto, M. *Biochem. Eng. J.* **2010**, *48*, 295–314.
(9) Stark, A.; Ajam, M.; Green, M.; Rabenheimer, H. G.; Ranwell, A.; Ondruschka, B. *Adv. Synth. Catal.* **2006**, *348*, 1934–1941.
(10) Hu, X.; Lin, Q.; Gao, J.; Wu, Y.; Zhang, Z. *Chem. Phys. Lett.* **2011**, *516*, 35–39.
(11) Isaacs, N. S. *Physical Organic Chemistry*, 1st ed.; Longman Scientific & Technical: New York, 1987.
(12) Tubbs, J. D.; Hoffmann, M. M. *J. Solution Chem.* **2004**, *33*, 381–394.
(13) Hayamizu, K.; Tsuzuki, S.; Seki, S.; Fujii, K.; Suenaga, M.; Umebayashi, Y. *J. Chem. Phys.* **2010**, *133*, 194505/194501–194505/194513.
(14) Tokuda, H.; Hayamizu, K.; Ishii, K.; Susan, M. A. B. H.; Watanabe, M. *J. Phys. Chem. B* **2004**, *108*, 16593–16600.
(15) Macchioni, A.; Ciancaleoni, G.; Zuccaccia, C.; Zuccaccia, D. *Chem. Soc. Rev.* **2008**, *37*, 479–489.
(16) May, H. O.; Mausbach, P. *Phys. Rev. E* **2007**, 76.
(17) Schmidt, J. R.; Skinner, J. L. *J. Phys. Chem. B* **2004**, *108*, 6767–6771.
(18) Liu, J.; Cao, D.; Zhang, L. *J. Phys. Chem. C* **2008**, *112*, 6653–6661.

(19) Sokolovskii, R. O.; Thachuk, M.; Patey, G. N. *J. Chem. Phys.* **2006**, *125*, 204502.
(20) Cappelezzo, M.; Capellari, C. A.; Pezzin, S. H.; Coelho, L. A. F. *J. Chem. Phys.* **2007**, *126*, 224516.
(21) Chen, B.; Sigmund, E.; Halperin, W. *Phys. Rev. Lett.* **2006**, *96*, 145502.
(22) Kumar, P. *Proc. Natl. Acad Sci. U.S.A.* **2006**, *103*, 12955−12956.
(23) Ediger, M. D. *Annu. Rev. Phys. Chem.* **2000**, *51*, 99−128.
(24) Mazza, M.; Giovambattista, N.; Stanley, H.; Starr, F. *Phys. Rev. E* **2007**, *76*, 031203.
(25) Kowert, B. A.; Watson, M. B. *J. Phys. Chem. B* **2011**, *115*, 9687−9694.
(26) Kowert, B. A.; Jones, J. B.; Zahm, J. A.; Turner, R. M. *Mol. Phys.* **2004**, *102*, 1489−1497.
(27) Del Popolo, M.; Voth Gregory, A. *J. Phys. Chem. B* **2004**, *108*, 1744−1752.
(28) Weingärtner, H. *Angew. Chem., Int. Ed.* **2008**, *47*, 654−670.
(29) Köddermann, T.; Ludwig, R.; Paschek, D. *ChemPhysChem* **2008**, *9*, 1851−1858.
(30) Stark, A.; Zidell, A. W.; Hoffmann, M. M. *J. Mol. Liq.* **2011**, *160*, 166−179.
(31) Lovelock, K. R. J.; Ejigu, A.; Loh, S. F.; Men, S.; Licence, P.; Walsh, D. A. *Phys. Chem. Chem. Phys.* **2011**, *13*, 10155−10164.
(32) Kind, R.; Liechti, O.; Korner, N.; Hulliger, J.; Dolinsek, J.; Blinc, R. *Phys. Rev. B* **1992**, *45*, 7697−7703.
(33) Kato, H.; Saito, T.; Nabeshima, M.; Shimeda, K.; Kinugasa, S. *J. Magn. Reson.* **2006**, *180*, 266−273.
(34) Van Geet, A. L. *Anal. Chem.* **1968**, *40*, 2227−2229.
(35) Antalek, B. *Concepts Magn. Reson.* **2002**, *14*, 225−258.
(36) Jerschow, A.; Mueller, N. *J. Magn. Reson. A* **1996**, *123*, 222−225.
(37) Jerschow, A.; Mueller, N. *J. Magn. Reson.* **1997**, *125*, 372−375.
(38) Nicolay, K.; Braun, K. P. J.; de Graaf, R. A.; Dijkhuizen, R. M.; Kruiskamp, M. J. *NMR Biomed.* **2001**, *14*, 94−111.
(39) Clarà, R. A.; Gómez Marigliano, A. C.; Morales, D.; Sólimo, H. N. *J. Chem. Eng. Data* **2010**, *55*, 5862−5867.
(40) Lide, D. R. *CRC Handbook of Chemistry and Physics*, 83rd ed.; CRC Press: Boca Raton, FL, 2003.
(41) Cornellas, A.; Perez, L.; Comelles, F.; Ribosa, I.; Manresa, A.; Garcia, M. T. *J. Colloid Interface Sci.* **2011**, *355*, 164−171.
(42) Logotheti, G.-E.; Ramos, J.; Economou, I. G. *J. Phys. Chem. B* **2009**, *113*, 7211−7224.
(43) Fujii, K.; Kanzaki, R.; Takamuku, T.; Kameda, Y.; Kohara, S.; Kanakubo, M.; Shibayama, M.; Ishiguro, S.-i.; Umebayashi, Y. *J. Chem. Phys.* **2011**, *135*, 244502.
(44) Zhao, W.; Leroy, F.; Heggen, B.; Zahn, S.; Kirchner, B.; Balasubramanian, S.; Müller-Plathe, F. *J. Am. Chem. Soc.* **2009**, *131*, 15825−15833.
(45) Schulz, P. S.; Schneiders, K.; Wasserscheid, P. *Tetrahedron: Asymmetry* **2009**, *20*, 2479−2481.
(46) Vorotyntsev, M. A.; Zinovyeva, V. A.; Picquet, M. *Electrochim. Acta* **2010**, *55*, 5063−5070.
(47) Canongia Lopes, J. N.; Shimizu, K.; Padua, A. A. H.; Umebayashi, Y.; Fukuda, S.; Fujii, K.; Ishiguro, S.-i. *J. Phys. Chem. B* **2008**, *112*, 9449−9455.
(48) Fujii, K.; Fujimori, T.; Takamuku, T.; Kanzaki, R.; Umebayashi, Y.; Ishiguro, S.-I. *J. Phys. Chem. B* **2006**, *110*, 8179−8183.
(49) Tsuzuki, S.; Matsumoto, H.; Shinoda, W.; Mikami, M. *Phys. Chem. Chem. Phys.* **2011**, *13*, 5987−5993.
(50) Chen, H.-C.; Chen, S.-H. *J. Phys. Chem.* **1984**, *88*, 5118−5121.
(51) Gierer, A.; Wirtz, K. *Z. Naturforsch. A* **1953**, *8*, 532−538.
(52) Zuccaccia, D.; Maccioni, A. *Organometallics* **2005**, *24*, 3476−3486.
(53) Fitchett, B. D.; Knepp, T. N.; Conboy, J. C. *J. Electrochem. Soc.* **2004**, *151*, E219−E225.
(54) Bulut, S.; Eiden, P.; Beichel, W.; Slattery, J. M.; Beyersdorff, T. F.; Schubert, T. J. S.; Krossing, I. *ChemPhysChem* **2011**, *12*, 2296−2310.
(55) Stolwijk, N. A.; Obeidi, S. *Electrochim. Acta* **2009**, *54*, 1645−1653.
(56) Rodriguez, V.; Grondin, J.; Adamietz, F.; Danten, Y. *J. Phys. Chem. B* **2010**, *114*, 15057−15065.
(57) Kolbeck, C.; Lehmann, J.; Lovelock, K. R. J.; Cremer, T.; Paape, N.; Wasserscheid, P.; Froba, A. P.; Maier, F.; Steinruck, H. P. *J. Phys. Chem. B* **2010**, *114*, 17025−17036.
(58) Klomfar, J.; Souckova, M.; Patek, J. *J. Chem. Thermodyn.* **2010**, *42*, 323−329.
(59) Carvalho, P. J.; Neves, C. M. S. S.; Coutinho, J. A. P. *J. Chem. Eng. Data* **2010**, *55*, 3807−3812.
(60) Fernandes, A. M.; Rocha, M. A. A.; Freire, M. G.; Marrucho, I. M.; Coutinho, J. A. P.; Santos, L. M. N. B. F. *J. Phys. Chem. B* **2011**, *115*, 4033−4041.
(61) Kato, R.; Gmehling, J. *J. Chem. Thermodyn.* **2005**, *37*, 603−619.
(62) Tokuda, H.; Tsuzuki, S.; Susan, M. A. B. H.; Hayamizu, K.; Watanabe, M. *J. Phys. Chem. B* **2006**, *110*, 19593−19600.
(63) Kumelan, J.; Tuma, D.; Maurer, G. *Fluid Phase Equilib.* **2009**, *275*, 132−144.
(64) Widegren Jason, A.; Magee Joseph, W. *J. Chem. Eng. Data* **2007**, *52*, 2331−2338.
(65) Kandil, M. E.; Marsh, K. N.; Goodwin, A. R. H. *J. Chem. Eng. Data* **2007**, *52*, 2382−2387.
(66) Muhammad, A.; Mutalib, M. I. A.; Wilfred, C. D.; Murugesan, T.; Shafeeq, A. *J. Chem. Thermodyn.* **2008**, *40*, 1433−1438.
(67) Ahosseini, A.; Sensenich, B.; Weatherley, L. R.; Scurto, A. M. *J. Chem. Eng. Data* **2010**, *55*, 1611−1617.
(68) Gonzalez, E. J.; Dominguez, A.; Macedo, E. A. *J. Chem. Thermodyn.* **2012**, *47*, 300−311.
(69) Singh, T.; Kumar, A. *J. Phys. Chem. B* **2007**, *111*, 7843−7851.
(70) Huang, M.-M.; Jiang, Y.; Sasisanker, P.; Driver, G. W.; Weingartner, H. *J. Chem. Eng. Data* **2011**, *56*, 1494−1499.
(71) Jiang, Y.; Nadolny, H.; Kaeshammer, S.; Weibels, S.; Schröer, W.; Weingärtner, H. *Faraday Discuss.* **2012**, *154*, 391−407.
(72) Shimomura, T.; Fujii, K.; Takamuku, T. *Phys. Chem. Chem. Phys.* **2010**, *12*, 12316−12324.
(73) Schneiders, K.; Bösmann, A.; Schulz, P. S.; Wasserscheid, P. *Adv. Synth. Catal.* **2009**, *351*, 432−440.
(74) Taylor, A. W.; Licence, P.; Abbott, A. P. *Phys. Chem. Chem. Phys.* **2011**, *13*, 10147−10154.
(75) Fendler, J. H. *Membrane Mimetic Chemistry*; Wiley: New York, 1982.